

The Role of Acridin-9(10H)-one in the Inhibition of Carbon Steel Corrosion: Thermodynamic, Electrochemical and DFT Studies

A. H. Al Hamzi¹, H. Zarrok², A. Zarrouk^{3, *}, R. Salghi⁶, B. Hammouti³, S. S. Al-Deyab⁵,
M. Bouachrine⁴, A. Amine¹, F. Guenoun¹

¹ Laboratoire Chimie – Biologie Appliquées à l'Environnement, Equipe CMMBA, Université Moulay Ismail, Faculté des Sciences, Meknès, Morocco.

² Laboratoire des procédés de séparation, Faculté des Sciences, Université Ibn Tofail, Kénitra, Morocco.

³ LCAE-URAC18, Faculté des Sciences, Université Mohammed 1^{er}, Oujda, Morocco.

⁴ ESTM, Université Moulay Ismail, Meknes, Morocco.

⁵ Petrochemical Research Chair, Chemistry Department, College of Science, King Saud University, P.O. Box 2455, Riyadh 11451, Saudi Arabia.

⁶ Equipe de Génie de l'Environnement et Biotechnologie, ENSA, Université Ibn Zohr, BP1136 Agadir, Morocco.

*E-mail: azarrouk@gmail.com

Received: 21 November 2012 / *Accepted:* 12 December 2012 / *Published:* 1 February 2013

Inhibition of the corrosion of carbon steel in aerated 1.0 M HCl solution by acridin-9(10H)-one (Hydacr) was investigated by use of gravimetric, potentiodynamic polarization (Tafel) and electrochemical impedance spectroscopy. Quantum chemical data were calculated by use of the density functional theory (DFT) model. Potentiodynamic polarization measurements clearly reveal that the investigated inhibitor is of mixed type, and it inhibits the corrosion of the steel by blocking the active site of the metal. Changes in impedance parameters were indicative of adsorption of Hydacr on the metal surface, leading to the formation of protective films. Thermodynamic parameters led to the conclusion that adsorption is predominantly chemisorption. Quantum chemical calculations were carried out to investigate the corrosion-inhibiting property of Hydacr. Various parameters such as energy of the highest occupied molecular orbital (HOMO) and lowest unoccupied molecular orbital (LUMO), softness of molecule were calculated and correlated with the inhibiting property of Hydacr.

Keywords: Acridone, Steel, Corrosion inhibition, Electrochemical techniques, DFT.

1. INTRODUCTION

Corrosion is a fundamental process playing an important role in economics and safety, particularly for metals and alloys. Steel has found wide application in a broad spectrum of industries and machinery; however, it has a tendency to corrode. The corrosion of steel is of fundamental academic and industrial concern which has received a considerable amount of attention [1]. Acid solutions are widely used in industry, some of the important fields of application being acid pickling of steel, chemical cleaning and

processing, ore production, and oil well acidizing. As an acidic medium, hydrochloric acid is more economical, efficient and trouble-free compared to other mineral acids [2]. Organic compounds containing nitrogen, sulphur, and oxygen are usually used as inhibitors against the corrosion of metals in acidic media [3-23].

The adsorption on the steel surface is carried out and the adsorption takes place through the nitrogen heteroatom as well as those with triple or conjugated double bonds or aromatic rings in their molecular structures. Also, it is generally accepted that the adsorption of the inhibitor on the steel/solution interface is affected by the chemical structures of the inhibitors, the nature of the charged surface of the metal, and the distribution of the charge over the whole inhibitor molecule [24]. The synthesized acridin-9(10*H*)-one derivative has additional π - bonds as well as N and O heteroatoms, which are assumed to be the active center of adsorption. Therefore, the molecule is expected to show better adsorption ability and corrosion inhibition efficiency.

The aim of this study is to investigate the inhibition efficiency of the synthesized acridin-9(10*H*)-one (Hydacr) on the carbon steel surface in 1.0 M HCl solution. For this purpose, weight loss (WL), potentiodynamic polarization (PP), and electrochemical impedance spectroscopy techniques were used. The adsorption isotherm of inhibitor on steel surface was determined. Both standard thermodynamic parameters and kinetic parameters are calculated and discussed in detail. Also, the purpose of the present work is to discuss the relationship between the quantum chemical calculations and the experimental protection efficiencies of the tested inhibitor by determining various quantum chemical parameters using DFT method. The chemical structure of the studied Hydacr derivative is given in Fig 1.

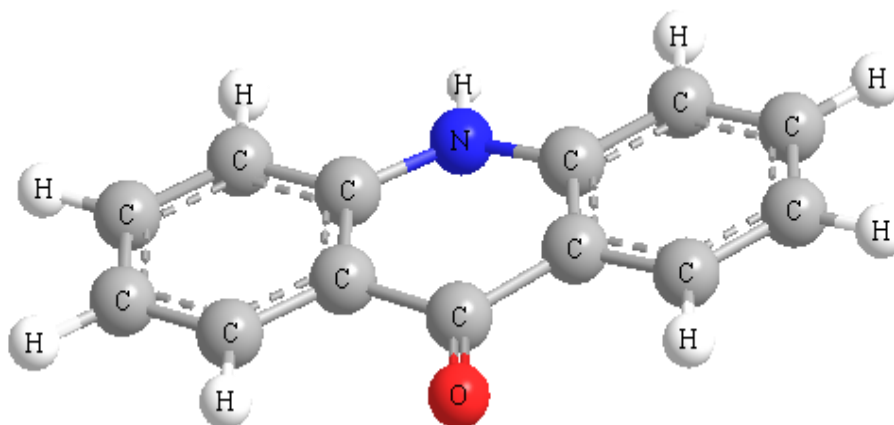


Figure 1. The chemical structure of the studied acridin-9(10*H*)-one compound.

2. EXPERIMENTAL METHODS

2.1. Materials

The steel used in this study is a carbon steel (Euronorm: C35E carbon steel and US specification: SAE 1035) with a chemical composition (in wt%) of 0.370 % C, 0.230 % Si, 0.680 % Mn, 0.016 % S, 0.077 % Cr, 0.011 % Ti, 0.059 % Ni, 0.009 % Co, 0.160 % Cu and the remainder iron (Fe). The carbon steel samples were pre-treated prior to the experiments by grinding with emery paper SiC (120, 600 and 1200); rinsed with distilled water, degreased in acetone in an ultrasonic bath immersion for 5 min, washed again with bidistilled water and then dried at room temperature before use. The acid solutions (1.0 M HCl) were prepared by dilution of an analytical reagent grade 37 % HCl with double-distilled water. The concentration range of Hydacr employed was 10^{-6} M to 10^{-3} M.

2.2. Synthesis

Acridin-9(10H)-one was prepared in two steps using Ullmann condensation [25].

Synthesis of 2-(phenylamino)benzoic acid (1)

A mixture of *o*-bromobenzoic acid 3.7 g (0.0184 mol), aniline 6.4 g (0.0688 mol), anhydrous potassium carbonate 3.0 g, copper 0.15 g and copper oxide 0.075 g in isoamylic alcohol (25 ml) is refluxed for 4 h. The mixture is allowed to stand at room temperature and the reaction mixture is poured into 200 ml of water. A precipitate is formed; the pH of the solution is made acidic with conc. HCl. The precipitate is filtered and washed with hot water thoroughly. The collected precipitate is dissolved in aqueous sodium hydroxide solution and heated with activated charcoal and filtered. The solution is then acidified with conc. HCl. A white colored precipitate is formed. It is filtered, washed again with hot water and dried. (mp 181 °C, 62%)

Synthesis of acridin-9(10H)-one

The cyclization of 1 in refluxing polyphosphoric acid (PPA) led to the acridin-9(10H)-one 2 by an intra-molecular Friedel-Crafts acylation [26]. Compound 1 (5 g, 0.023 mol) was placed in a round bottom flask with poly phosphoric acid (25 ml), shaken well and heated on water bath at 180 °C for 3 h. The mixture is poured into hot water (150 ml). Acridin-9(10H)-one is collected as a yellow precipitate, washed with water and dried. (mp > 300 °C, 74%)

2.3. Measurements

2.3.1. Weight loss measurements

The steel sheets of $1.6 \times 1.6 \times 0.07$ cm dimensions were abraded with different grades of emery papers, washed with distilled water, degreased with acetone, dried and kept in a desiccator. After weighing accurately by a digital balance with high sensitivity the specimens were immersed in solution containing 1.0 M HCl solution with and without various concentrations of the investigated inhibitor. At the end of the tests, the specimens were taken out, washed carefully in ethanol under ultrasound

until the corrosion products on the surface of carbon steel specimens were removed thoroughly, and then dried, weighed accurately. Duplicate experiments were performed in each case and the mean value of the weight loss is reported. Weight loss allowed calculation of the mean corrosion rate in $\text{mg cm}^{-2} \text{h}^{-1}$. The corrosion rate (v) and the inhibition efficiency (η) were calculated by the following equations:

$$v = \frac{W}{St} \times 100 \quad (1)$$

$$\eta(\%) = \frac{v_0 - v}{v_0} \times 100 \quad (2)$$

where W is the three-experiment average weight loss of the carbon steel, S is the total surface area of the specimen, t is the immersion time and v_0 and v are values of the corrosion rate without and with addition of the inhibitor, respectively.

2.3.2. Electrochemical measurements

The electrochemical measurements were carried out using Volta lab (Tacussel- Radiometer PGZ 100) potentiostat and controlled by Tacussel corrosion analysis software model (Voltmaster 4) at under static condition. The corrosion cell used had three electrodes. The reference electrode was a saturated calomel electrode (SCE). A platinum electrode was used as auxiliary electrode of surface area of 1 cm^2 . The working electrode was carbon steel. All potentials given in this study were referred to this reference electrode. The working electrode was immersed in test solution for 30 minutes to establish steady state open circuit potential (E_{ocp}). After measuring the E_{ocp} , the electrochemical measurements were performed. All electrochemical tests have been performed in aerated solutions at 308 K. The polarization curves were obtained in the potential range from -800 to -200 mV(SCE) with 1 mV s^{-1} scan rate. The EIS experiments were conducted in the frequency range with high limit of 100 kHz and different low limit 0.1 Hz at open circuit potential, with 10 points per decade, at the rest potential, after 30 min of acid immersion, by applying 10 mV ac voltage peak-to-peak. Nyquist plots were made from these experiments. The best semicircle can be fit through the data points in the Nyquist plot using a non-linear least square fit so as to give the intersections with the x -axis.

2.3.3. Quantum chemical calculations

All theoretical calculations were performed using DFT (density functional theory) with the Beck's three parameter exchange functional along with the Lee-Yang-Parr nonlocal correlation functional (B3LYP) [27-29] with 6-31G* basis set is implemented in Gaussian 03 program package [30]. This approach is shown to yield favorable geometries for a wide variety of systems. The following quantum chemical parameters were calculated from the obtained optimized molecular

structure: the energy of the highest occupied molecular orbital (E_{HOMO}), the energy of the lowest unoccupied molecular orbital (E_{LUMO}), the energy band gap ($\Delta E_{\text{gap}} = E_{\text{HOMO}} - E_{\text{LUMO}}$), the dipole moment (μ), the electron affinity (A), the ionization potential (I) and softness were calculated and discussed.

3. RESULTS AND DISCUSSION

3.1. Polarization curves

The representative potentiodynamic polarization curves of carbon steel in 1.0 M HCl solution in the absence and presence of various concentrations of Hydacr are shown in Fig. 2. As it can be seen from Fig. 2, both cathodic and anodic reactions are inhibited after the addition of Hydacr to the aggressive solution, and this inhibition more and more pronounced with increasing inhibitor concentration. Corrosion potential (E_{corr}) of carbon steel Remains almost unchanged in the presence of Hydacr when it is compared to that observed in blank solution. These results show that the addition of Hydacr to the corrosive solution both reduce the anodic dissolution of carbon steel and also retard the hydrogen evolution reaction. Cathodic current potential curves give rise to parallel Tafel lines indicates that the hydrogen evolution reaction is activation-controlled and the reduction of H^+ ions at the carbon steel surface occur mainly through a charge transfer mechanism [31]. The addition of Hydacr to 1.0 M HCl solution does not affect the mechanism. This means that the inhibition of hydrogen evolution reaction takes place by adsorption mode, a and the mechanism is the same with and without the inhibitor.

Table 1 shows the electrochemical parameters of carbon steel determined from polarization measurements, i.e., corrosion potential (E_{corr}), cathodic Tafel slope (β_c), corrosion current density (I_{corr}), corrosion rate (CR) and inhibition efficiency ($E_I\%$). i_{corr} values were determined by extrapolation of Tafel lines to the corresponding corrosion potentials. The inhibition efficiency $E_I\%$, was calculated from polarization measurements according to following equation:

$$E_I (\%) = \frac{I_{\text{corr}} - I_{\text{corr(inh)}}}{I_{\text{corr}}} \times 100 \quad (3)$$

where I_{corr} and $I_{\text{corr(inh)}}$ are the corrosion current densities for steel electrode in the uninhibited and inhibited solutions, respectively.

It is clear from Table 1 that, the i_{corr} value decreases and $E_I\%$ increased with increasing inhibitor concentration, whereas the cathodic Tafel slopes nearly remains the same indicates the adsorption of Hydacr molecules on the steel surface and impedes by merely blocking the reaction sites of surface without affecting the cathodic reaction mechanisms [32]. A compound is usually classified as an anodic or a cathodic type inhibitor when the change in E_{corr} value is larger than 85 mV [33, 34]. Since the small displacement of the corrosion potential was about 8.7 mV (Table 1) after the addition of the Hydacr, suggesting that the inhibitor acted as a mixed-type inhibitor.

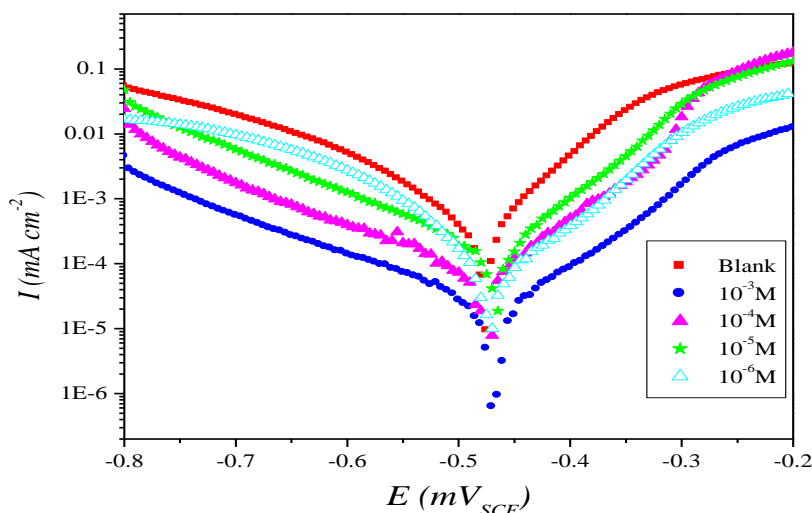


Figure 2. Polarisation curves of carbon steel in 1.0 M HCl for various concentrations of Hydacr.

Table 1. Polarization data of carbon steel in 1.0 M HCl without and with addition of inhibitor at 308 K.

Inhibitor	Conc (M)	$-E_{\text{corr}}$ (mV/SCE)	$-\beta_c$ (mV dec ⁻¹)	I_{corr} ($\mu\text{A cm}^{-2}$)	E_I (%)
HCl	1	475.9	176.0	1077.8	-
Hydacr	10^{-3}	468.9	166.6	24.1	97.8
	10^{-4}	474.1	165.0	66.9	93.8
	10^{-5}	467.2	156.9	137.4	86.4
	10^{-6}	473.0	125.6	259.0	74.9

3.2. Electrochemical impedance spectroscopy

All impedance measurements were performed under potentiostatic conditions after immersion for 0.5 h. Simulation of bode plot with above model shows excellent agreement with experimental data (Fig. 3, representative example). The Nyquist diagrams have similar shapes for different concentrations of the inhibitor molecule. The mechanism of corrosion remains unaffected during addition of inhibitor molecules. The simplest fit is represented by the Randles equivalent circuit, Fig. 4, which is a parallel combination of the charge-transfer resistance (R_{ct}) and the constant phase element (CPE) [35], both in series with the solution resistance (R_s). The impedance spectra contain one single depressed semicircle, and the diameter of the semicircle increases with increasing inhibitor concentration. The single semicircle indicates that charge transfer takes place at electrode/electrolyte interface, and the corrosion reaction of steel is controlled by the transfer process [36]. Also, these impedance diagrams are not perfect semicircles; this is related to the frequency dispersion as a result of the roughness and inhomogeneity of the electrode surface [37]. Furthermore, the impedance response of the rate of corrosion in uninhibited solution changed significantly after addition of inhibitor to the

corrosive solution; as a result, the real axis intercept at high and low frequencies in the presence of the inhibitor is larger than that in the absence of inhibitor (blank solution) and increases with the inhibitor concentration. The capacitive loop corresponds to the charge transfer reaction, which depends on either direct electron transfer at the metal surface or on electron conduction through the film surface. The impedance diagrams (Nyquist) contain depressed semicircles with the center under the real axis. Such behavior is characteristic of solid electrodes and is attributed to different physical phenomena, for example roughness, inhomogeneities of the solid surfaces, impurities, grain boundaries, and distribution of surface active sites. In this case, the CPE is used in the circuit instead of a pure double-layer capacitor to give a more accurate fit [38, 39]. The equation of the impedance function of a CPE is:

$$Z_{CPE} = A^{-1} (CE)^{-n} \tag{4}$$

where A is the CPE constant (in $\Omega^{-1} S^n cm^{-2}$), E is the sine wave modulation angular frequency (rad^{-1}), $i^2 = -1$ is the imaginary number, and α is an empirical exponent ($0 \leq n \leq 1$), which measures the deviation from ideal capacitive behavior [40, 41].

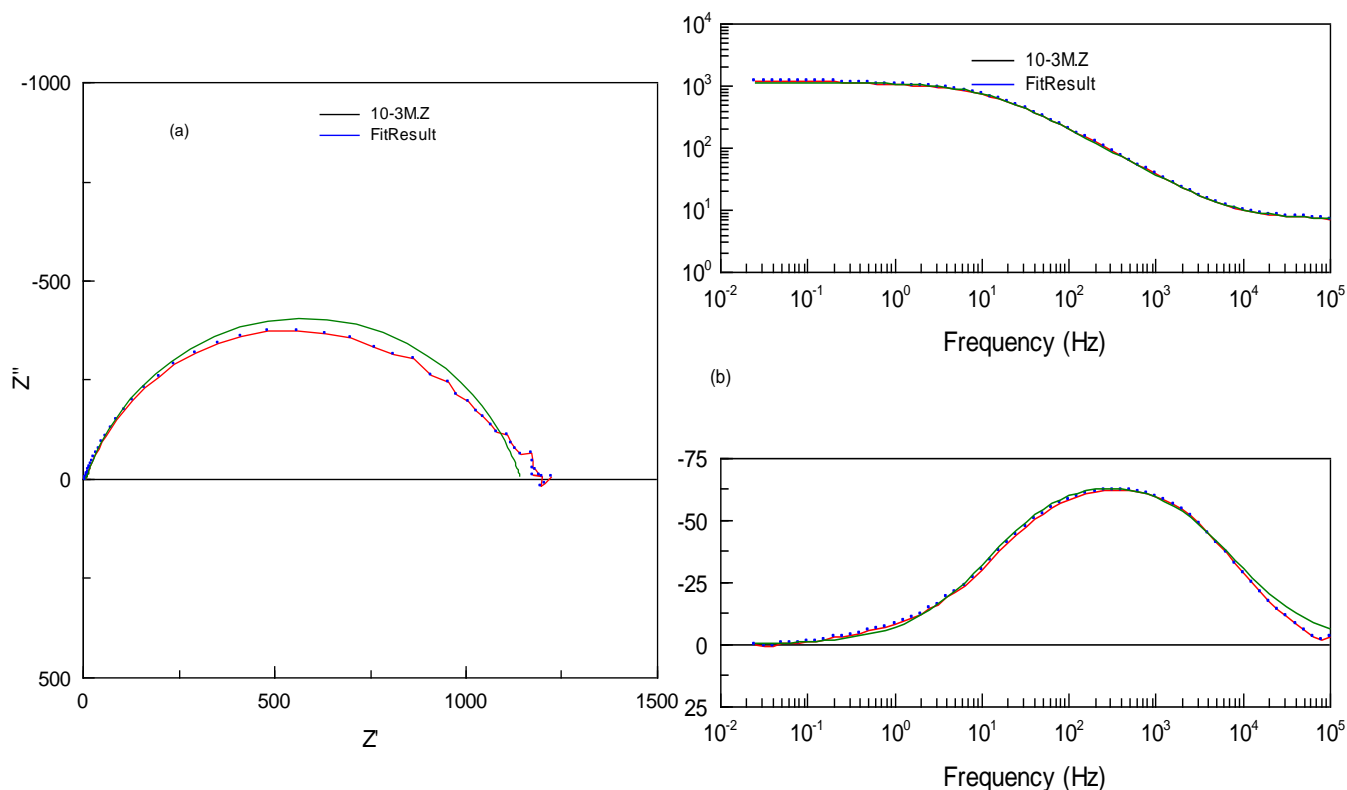


Figure 3. EIS Nyquist (a) and Bode (b) plots for carbon steel/1.0 M HCl + 10^{-3} M Hydacr interface: dotted lines experimental data; dashed line calculated.

The inhibition efficiencies at different inhibitor concentrations were calculated by use of the equation:

$$IE_{R_{ct}}(\%) = \frac{R_{ct(inh)} - R_{ct}}{R_{ct(inh)}} \times 100 \tag{5}$$

where R_{ct} and $R_{ct(inh)}$ are the charge transfer resistance values in absence and presence of inhibitor for carbon steel in 1.0 M HCl, respectively [42].

The opposite trend in the values of R_{ct} and C_{dl} (Table 2) over the whole concentration range can be assumed to be because of the formation of a protective layer which covers the whole surface of the electrode. The impedance values are given in Table 2. The charge-transfer resistance is increased from 29.66 for inhibitor-free solution to 1136 $\Omega\text{ cm}^2$ on addition of 10^{-3} M Hydacr, resulting in 97.4% inhibition efficiency. The increase in R_{ct} is attributed to the formation of an insulating protective film at the metal/solution interface [43, 44]. The double-layer capacitance decreases from 85.31 to 11.54 $\mu\text{F cm}^{-2}$ in the presence of 10^{-3} M Hydacr. The initial decrease in C_{dl} from blank solution to inhibitor-containing electrolyte is because of a decrease in the local dielectric constant, and the further decrease in C_{dl} with increasing concentrations of the inhibitor is because of the increase in the thickness of the electrical double layer.

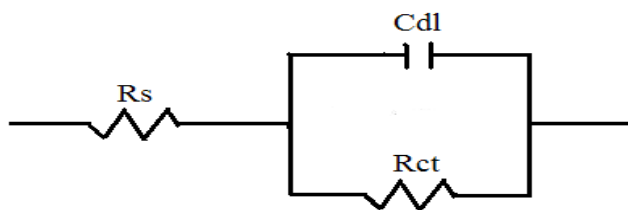


Figure 4. Equivalent circuit used to fit the EIS data for carbon steel and different inhibitor concentrations.

Table 2. Impedance parameters for corrosion of steel in 1.0 M HCl in the absence and presence of different concentrations of Hydacr at 308 K.

Conc (M)	R_s ($\Omega\text{ cm}^2$)	R_{ct} ($\Omega\text{ cm}^2$)	n	$A \times 10^{-4}$ ($\text{s}^n \Omega^{-1} \text{cm}^{-2}$)	C_{dl} ($\mu\text{F cm}^{-2}$)	$IE_{R_{ct}}$ (%)
Blank	1.67	29.66	0.91	0.14612	85.31	-----
10^{-3}	7.06	1136	0.79	0.28685	11.54	97.4
10^{-4}	0.71	405.5	0.84	0.67292	33.89	92.7
10^{-5}	10.3	199.2	0.88	0.70369	39.32	85.1
10^{-6}	7.52	110.1	0.90	0.85693	51.04	73.1

3.3. Gravimetric study

3.3.1. Effect of concentration inhibitor

Gravimetric measurement which is a reliable and concise analytical method was also used for the study of the inhibitive effect of Hydacr under different concentrations [45,46]. To ensure the

reproducibility, experiments were performed for three times and the average results are compiled in Table 3. Clearly, with gradually increased inhibitor concentrations the weight loss as well as the corrosion rate (v) of the carbon steel diminished distinctly, which is in agreement with the results obtained by EIS. An excellent inhibitory efficiency (η) assigning to 98.3% was acquired at the highest inhibitor concentration applied (10^{-3} M). On the other hand, the high η % values found indicate a strong adsorption favored by the long duration of the experiments. Therefore, the weight loss experiments confirmed the electrochemical results regarding the adsorption of this compound on the carbon steel surface forming a protective film barrier.

Table 3. Corrosion parameters obtained from weight loss measurements for carbon steel in 1.0 M HCl containing various concentration of inhibitor at 308 K.

Inhibitor	Conc (M)	v (mg/cm ² h)	η (%)	θ
Blank	1	1.070	-----	-----
Hydacr	1×10^{-3}	0.018	98.3	0.983
	1×10^{-4}	0.059	94.5	0.945
	1×10^{-5}	0.139	87.0	0.870
	1×10^{-6}	0.256	76.1	0.761

3.3.2. Effect of temperature

The effect of temperature on the corrosion rate of carbon steel in 1.0 M HCl over the temperature range (308 to 333K) (see Table 4) in the absence and presence of different concentrations of the investigated compounds has been studied. The % inhibition efficiency is found to decrease with increasing the temperature; this indicated that, these compounds are physically adsorbed on the carbon steel surfaces.

Plots of logarithm of corrosion rate ($\ln v$), with reciprocal of absolute temperature ($1/T$) for carbon steel in 1.0 M HCl at 1.0×10^{-3} M after 1h. for the used compounds are shown in (Fig. 5). As shown from this Figure, straight lines with slope of $-E_a/R$ and intercept of A were obtained according to Arrhenius-type equation:

$$v = A \exp\left(\frac{-E_a}{RT}\right) \quad (6)$$

where v is the corrosion rate, A is a constant depends on a metal type and electrolyte, E_a is the apparent activation energy, R is the universal gas constant and T is the absolute temperature. The fractional surface coverage θ can be easily determined from weight loss measurements by the ratio η % / 100 if one assumes that the values of η % do not differ substantially from θ .

Table 4. Various corrosion parameters for carbon steel in 1.0 M HCl in the absence and the presence of optimum concentration of Hydacr at different temperatures after 1h.

Temp (K)	Inhibitor	v (mg cm ⁻² h ⁻¹)	η (%)	θ
308	Blank	1.070	-----	-----
	Hydacr	0.018	98.3	0.983
313	Blank	1.490	-----	-----
	Hydacr	0.058	96.1	0.961
323	Blank	2.870	-----	-----
	Hydacr	0.221	92.3	0.923
333	Blank	5.210	-----	-----
	Hydacr	0.792	84.8	0.848

Plots of $\ln(v/T)$ vs. $1/T$ for carbon steel in 1.0 M HCl at 1.0×10^{-3} M after 1h. for the used compounds are shown in (Fig. 6). As shown from this Figure, straight lines with slope of $(-\Delta H_a / R)$ and intercept of $(\ln R / Nh + \Delta S_a / R)$ were obtained according to transition state equation [47]:

$$v = \frac{RT}{Nh} \exp\left(\frac{\Delta S_a}{R}\right) \exp\left(-\frac{\Delta H_a}{RT}\right) \quad (7)$$

where v is the corrosion rate, h is the Planck's constant (6.626176×10^{-34} Js), N is the Avogadro's number (6.02252×10^{23} mol⁻¹), R is the universal gas constant and T is the absolute temperature, ΔH_a the enthalpy of activation, and ΔS_a entropy of activation.

The calculated values of the apparent activation energy, E_a , activation enthalpies, ΔH_a and activation entropies, ΔS_a are given in Table 5. The increase in the activation energy in the presence of inhibitor indicates the higher inhibition efficiency of the inhibitor. Also the E_a value is 54.14 kJ mol⁻¹ which attributed to the physisorption of inhibitor on the metal surface [48-52]. The increase in E_a in case of the protected carbon steel with the addition of 1.0×10^{-3} M of this different inhibitor indicates that the energy barrier for the corrosion reaction increases. The increase in E_a of the corrosion process could be attributed to the adsorption of the inhibitor molecules onto the metal surface which decreases the interaction between the corrosive medium and the metal surface. The positive signs of ΔH_a reflect the endothermic nature of the carbon steel dissolution process [53]. The large negative value of ΔS_a for carbon steel in 1.0 M HCl implies that the activated complex is the rate-determining step, rather than the dissociation step. In the presence of the inhibitor, the value of ΔS_a increases and is generally interpreted as an increase in disorder as the reactants are converted to the activated complexes [54]. The positive values of ΔS_a reflect the fact that the adsorption process is accompanied by an increase in entropy, which is the driving force for the adsorption of the inhibitor onto the steel surface.

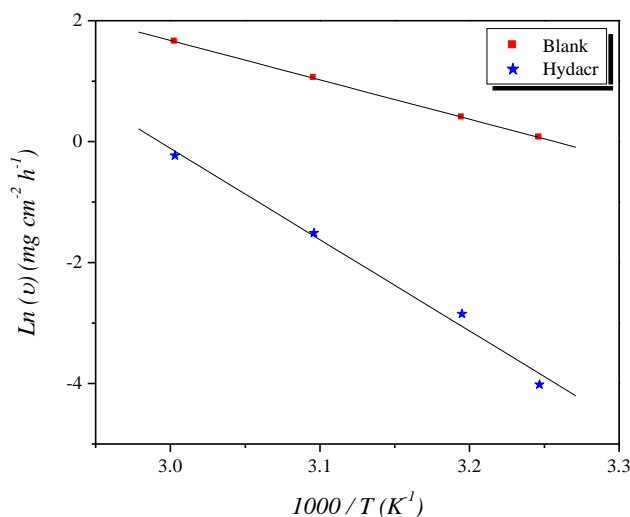


Figure 5. Arrhenius plots of Ln (v) vs. 1/T for steel in 1.0 M HCl in the absence and the presence of Hydacr at optimum concentration.

Table 5. Activation parameters for the steel dissolution in 1.0 M HCl in the absence and the presence of Hydacr at optimum concentration.

Inhibitor	A (mg cm ⁻² h ⁻¹)	Linear regression coefficient (r)	E _a (kJ/mol)	ΔH _a (kJ/mol)	ΔS _a (J/mol K)
Blank	1.6260×10 ⁹	0.99997	54.14	51.48	-77.49
Hydacr	4.0814×10 ¹⁹	0.99480	125.45	122.72	121.60

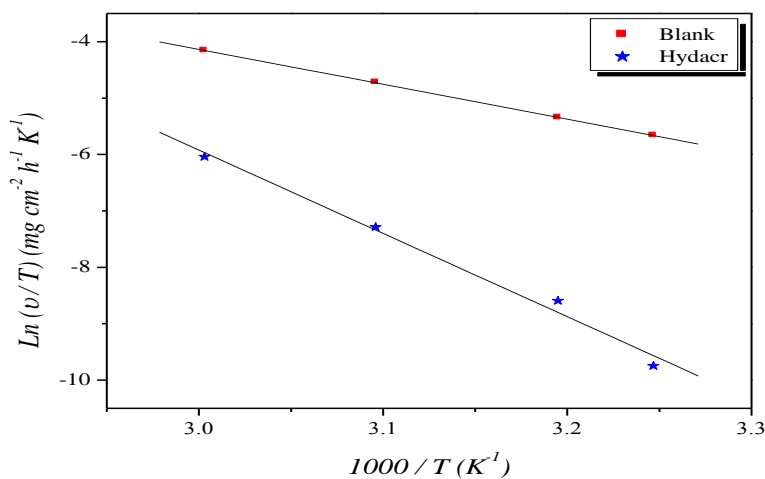


Figure 6. Arrhenius plots of Ln (v /T) vs. 1/T for steel in 1.0 M HCl in the absence and the presence of Hydacr at optimum concentration.

3.3.3. Adsorption isotherm

The extent of corrosion inhibition depends on the surface conditions and the mode of adsorption of the inhibitor [55]. Under the assumptions that corrosion of the covered parts of the surface is equal to zero and corrosion takes place only on the uncovered parts of the surface (i.e., inhibitor efficiency is mainly because of the blocking effect of the adsorbed species), the degree of surface coverage, θ , was estimated by use of the chemical and electrochemical techniques used in this study, as follows: $\theta = \eta (\%)/100$ (assuming a direct relationship between surface coverage and inhibition efficiency). Adsorption on the corroding surfaces never reaches real equilibrium and tends to reach an adsorption steady state. However, when the rate of corrosion is sufficiently small, the adsorption steady state has a tendency to become a quasi-equilibrium state. In this case, it is reasonable to consider the quasi-equilibrium adsorption thermodynamically using the appropriate equilibrium adsorption isotherms. Basic information on the interaction between the inhibitor and the carbon steel surface can be provided by the adsorption isotherm. To obtain the isotherm, the relationship between θ and inhibitor concentration (C_{inh}) must be found. Attempts were made to fit θ values to different isotherms (Langmuir, Temkin, Flory–Huggins, Dahar–Flory–Huggins, and Bockris–Swinkel isotherms [56, 57]). By far the best fit was obtained with the Langmuir isotherm (C_{inh} versus C_{inh} / θ); this is shown in Fig. 7. Adsorption of an organic substance at a metal/solution interface can be presented as a substitution adsorption process between the organic molecules in aqueous solution, (Org_{aq}), and the water molecules on the surface of the metal (H_2O_{ads}):



where x , the size ratio, is the number of water molecules displaced by one molecule of organic inhibitor. x is assumed to be independent of coverage or charge on the electrode [58]. To choose the appropriate isotherm describing the adsorption mechanism, the fraction of surface coverage (θ) was defined as $\eta (\%)/100$ and was obtained from electrochemical measurements at different temperatures. For inhibitor studies, it is found that gravimetric data can be fitted by the Langmuir model. According to this model, the surface coverage (θ) is proportional to inhibitor concentration (C_{inh}):

$$\frac{\theta}{1-\theta} = K_{ads} C_{inh} \quad (9)$$

By rearranging this equation:

$$\frac{C_{inh}}{\theta} = \frac{1}{K_{ads}} + C_{inh} \quad (10)$$

where K_{ads} is the adsorption constant, C_{inh} is the concentration of the inhibitor and surface coverage values (θ) are obtained from the weight loss measurements for various concentrations.

Figure 7 shows the C_{inh} / θ versus C_{inh} . The strong correlation coefficient 0.99999 indicates that adsorption of this inhibitor by carbon steel follows this isotherm and it was supposed that adsorbed molecules occupy one site only and there are no interactions with other adsorbed species. According to Eq. 10, K_{ads} can be calculated from intercept on the C_{inh} / θ axis. By use of the equation below, ΔG_{ads}° can be calculated from K_{ads}

$$\Delta G_{ads}^{\circ} = -RT \ln(55.5 K_{ads}) \quad (11)$$

Where R is gas constant and T is absolute temperature of experiment and the constant value of 55.5 is the concentration of water in solution in mol L⁻¹. The thermodynamics parameters derived from Langmuir adsorption isotherm for the studied compound, are given in Table 7. By use of Eq. 11, the calculated value of ΔG_{ads}° is -44.03 kJ mol⁻¹. The negative sign of ΔG_{ads}° demonstrates that the inhibitor is spontaneously adsorbed by the metal surface. Normally, a magnitude of ΔG_{ads}° of approximately -20 kJ mol⁻¹ or less negative is assumed for electrostatic interactions between inhibitor and the charged metal surface (i.e. physisorption). Values of approximately -40 kJ mol⁻¹ or more negative are indicative of charge sharing or transfer from the organic species to the metal surface to form a co-ordinate type of metal bond (i.e. chemisorption). Some authors have reported values of ΔG_{ads}° less negative than -40 kJ/mol for physical adsorption, for example formation of an adsorptive film with electrostatic character. The calculated standard free energy of adsorption value is closer to -40 kJ mol⁻¹. Therefore it can be concluded that the adsorption of the Hydacr on the carbon steel surface is more chemical than physical one. [59].

Table 7. Thermodynamic parameters for the adsorption of Hydacr in 1.0 M HCl on the carbon steel at 308K.

Inhibitor	Slope	K_{ads} (M ⁻¹)	R ²	ΔG_{ads}° (kJ/mol)	Q_{ads} (kJ/mol)
Hydacr	1.01	529753.61	0.99999	-44.03	-75.90

The heat of adsorption process (Q_{ads}) can also be estimated from the variation of the surface coverage with reciprocal of temperature by using Langmuir's adsorption isotherm as follows [60]:

$$\left[\frac{\theta}{1-\theta} \right] = A.C.\exp(-Q_{ads} / RT) \quad (12)$$

where A is a constant and Q_{ads} is the heat of adsorption which is almost equal to the enthalpy of adsorption (ΔH_{ads}°) [24]. A plot of $\ln [\theta / (1-\theta)]$ against $1/T$ is given in Figure 9. The value of heat of adsorption was determined from the slope ($-Q_{ads} / RT$) of the graph.

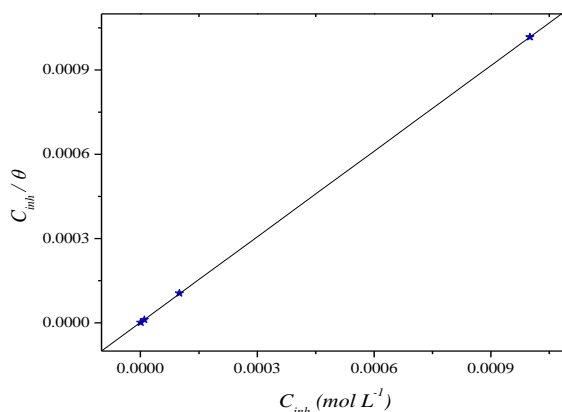


Figure 8. Langmuir adsorption of Hydacr on the carbon steel surface in 1.0 HCl solution.

The value of heat of adsorption is given in Table 7. It is evident from the Table 7 that (Q_{ads}) has negative value which indicates that inhibitor adsorption decreases with increase in the temperature hence decrease in inhibitor efficiency. The negative value of (Q_{ads}) also suggested that the adsorption of inhibitor is an exothermic process [61].

The entropy of inhibitor adsorption (ΔS_{ads}°) can be calculated using the following equation [62, 63]:

$$\Delta G_{ads}^\circ = \Delta H_{ads}^\circ - T\Delta S_{ads}^\circ \tag{13}$$

ΔS_{ads}° and ΔH_{ads}° values are -75.90 and 0.1035 kJ mol⁻¹, respectively. Valuable information about the mechanism of corrosion inhibition can be obtained from these thermodynamic data for the adsorption process.

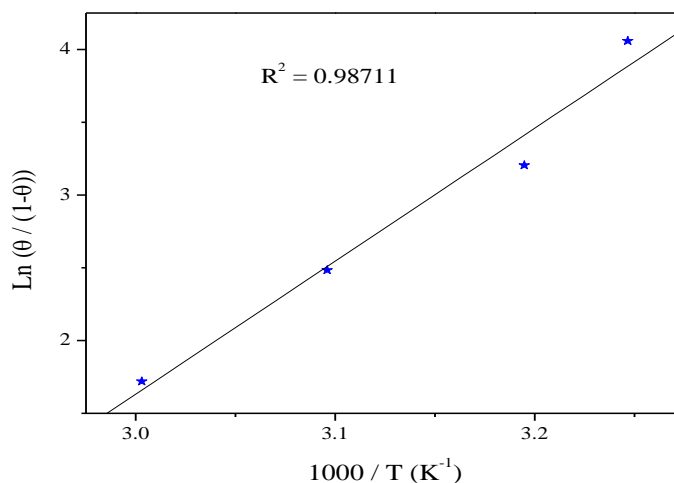


Figure 9. Ln ($\theta / (1 - \theta)$) vs.1/T for adsorption of Hydacr.

3.4. Quantum chemical calculations

Quantum chemical calculations have been widely used to study reaction mechanisms. They have also proved to be a very powerful tool for studying corrosion inhibition mechanisms [16, 64]. Recently, theoretical prediction of the efficiency of corrosion inhibitors has become very popular in parallel with the progress in computational hardware and the development of efficient algorithms which assisted the routine development of molecular quantum mechanical calculations [17, 65]. All quantum chemical properties were obtained after geometric optimization with respect to the all nuclear coordinates using Kohn-Sham approach at DFT level. The optimized structure of the studied compound as shown in Fig. 10.

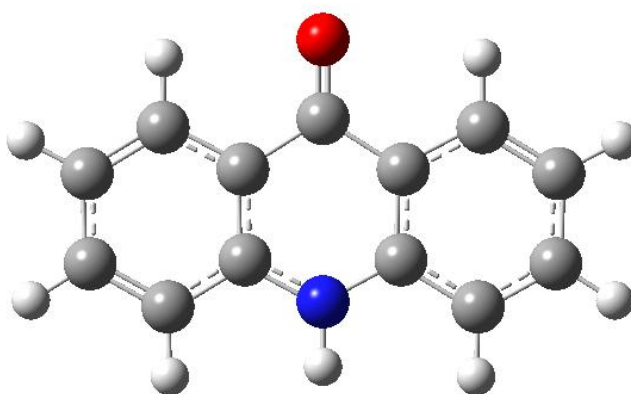
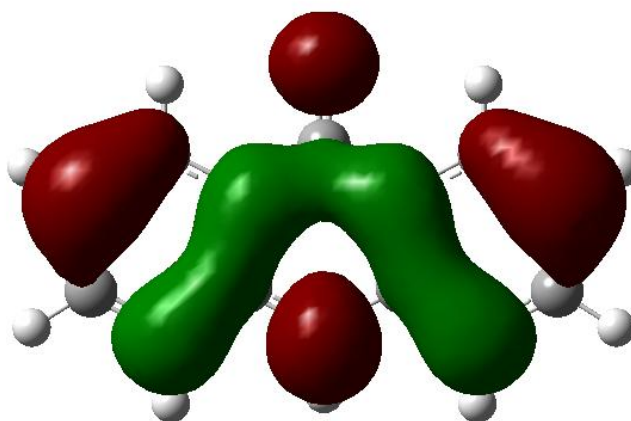


Figure 10. Optimized structure of studied molecule obtained by B3LYP/6-31G* level

In Fig. 11, we have presented the frontier molecule orbital density distributions of the studied compound. Analysis of Fig. 11 shows that the distribution of two energies HOMO and LUMO, we can see that the electron density of the HOMO and LUMO location was distributed almost of the entire molecule.



HOMO

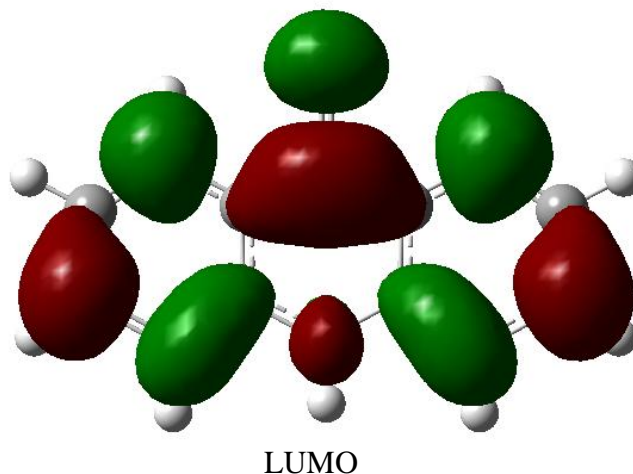


Figure 11. Schematic representation of HOMO and LUMO molecular orbital of studied molecule.

Table 8. Calculated quantum chemical parameters of the studied compound.

Quantum parameters	Hydacr
E_{HOMO} (eV)	-5.6202 eV
E_{LUMO} (eV)	-1.5074 eV
ΔE gap (eV)	4.1127 eV
μ (debye)	4.9531 debye
$I = -E_{HOMO}$ (eV)	5.6202 eV
$A = -E_{LUMO}$ (eV)	1.5074 eV
$\chi = \frac{I + A}{2}$ (eV)	3.5638
$\eta = \frac{I - A}{2}$ (eV)	2.0564
$\sigma = \frac{1}{\eta}$	0.4862
TE (eV)	-630.8120607 u.a

According to the frontier molecular orbital theory (FMO) of chemical reactivity, transition of electron is due to interaction between highest occupied molecular orbital (HOMO) and lowest unoccupied molecular orbital (LUMO) of reacting species [65]. E_{HOMO} is a quantum chemical parameter which is often associated with the electron donating ability of the molecule. High value of E_{HOMO} is likely to a tendency of the molecule to donate electrons to appropriate acceptor molecule of low empty molecular orbital energy [66]. The inhibitor does not only donate electron to the unoccupied d orbital of the metal ion but can also accept electron from the d-orbital of the metal leading to the formation of a feed back bond. The highest value of E_{HOMO} -5.6202 eV of the studied

compound indicates the better inhibition efficiency. On the other hand, It has also been found that an inhibitor does not only donate an electron to the unoccupied d orbital of the metal ion but can also accept electrons from the d orbital of the metal leading to the formation of a feedback bond. Therefore, the tendency for the formation of a feedback bond would depend on the value of E_{LUMO} . The lower value of the $E_{LUMO} = -1.5074$ eV indicates the easier of the acceptance of electrons from the d orbital of the metal [67-68]. The band gap energy, $\Delta E = E_{LUMO} - E_{HOMO}$ is an important parameter as a function of reactivity of the inhibitor molecule towards the adsorption on metallic surface. As ΔE decreases, the reactivity of the molecule increases leading to increase the inhibition efficiency of the molecule. The calculations indicate that our studied molecule has a small value of gap energy (4.1127 eV) which means the highest reactivity and accordingly the highest inhibition efficiency which agrees well with the experimental observations. Absolute hardness and softness are important properties to measure the molecular stability and reactivity. It is apparent that the chemical hardness fundamentally signifies the resistance towards the deformation or polarization of the electron cloud of the atoms, ions or molecules under small perturbation of chemical reaction. A hard molecule has a large energy gap and a soft molecule has a small energy gap [69]. In our present work the studied molecule has low hardness value 2.0564 (eV) and a highest value of softness of 0.4862

The most widely used quantity to describe the polarity is the dipole moment of the molecule [70]. Dipole moment is the measure of polarity of a polar covalent bond. It is defined as the product of charge on the atoms and the distance between the two bonded atoms. The total dipole moment, however, reflects only the global polarity of a molecule. For a complete molecule the total molecular dipole moment may be approximated as the vector sum of individual bond dipole moments. The dipole moment (μ in Debye) is another important electronic parameter that results from non uniform distribution of charges on the various atoms in the molecule. The high value of dipole moment probably increases the adsorption between chemical compound and metal surface [71]. In our study, the value of the dipole moment is 4.9531 debye.

The total energy calculated by quantum chemical methods is equal to -630.8120607 u.a. Hohenberg and Kohn [72] proved that the total energy of a system including that of the many body effects of electrons (exchange and correlation) in the presence of static external potential (for example, the atomic nuclei) is a unique functional of the charge density. The minimum value of the total energy functional is the ground state energy of the system. The electronic charge density which yields this minimum is then the exact single particle ground state energy.

4. CONCLUSION

1. Hydacr acts as a fairly good inhibitor for carbon steel in 1.0 M HCl solution.
2. The efficiency of inhibition by Hydacr increases with increasing concentration of the inhibitor, but decreases with increasing temperature.
3. Results obtained from polarization and ac impedance studies show that the percentage inhibition efficiency increases as concentration increases.
4. Polarization studies reveal that Hydacr act as a mixed-type inhibitor.

5. Adsorption of the inhibitor molecules on the metal surface fits Langmuir adsorption isotherm model.

6. The correlation between the quantum chemical parameters and inhibition efficiency was investigated using DFT/B3LYP calculations. The inhibition efficiency of the inhibitor are closely related to the quantum chemical parameters, the highest occupied molecular orbital (E_{HOMO}), energy of lowest unoccupied molecular orbital (E_{LUMO}), HOMO-LUMO energy gap ($\Delta E_{\text{H-L}}$), the hardness (σ), the softness (η), the dipole moment (μ) and the total energy (TE).

ACKNOWLEDGEMENTS

Prof S. S. Al-Deyab and Prof B. Hammouti extend their appreciation to the Deanship of Scientific Research at King Saud University for funding the work through the research group project.

References

1. A. K. Singh, M. A. Quraishi, *J. Mater. Environ. Sci.* 1 (2) (2010) 101.
2. D.D.N. Singh, T.B. Singh, B. Gaur, *Corros. Sci.* 37 (1995) 1005.
3. M. Prajila, J. Sam, J. Bincy, J. Abraham, *J. Mater. Environ. Sci.* 3 (6) (2012) 1045.
4. U.J. Naik, V.A. Panchal, A.S. Patel, N.K. Shah, *J. Mater. Environ. Sci.* 3 (5) (2012) 935.
5. A. Zarrouk, H. Zarrok, R. Salghi, B. Hammouti, F. Bentiss, R. Touir, M. Bouachrine, *J. Mater. Environ. Sci.* 4 (2) (2013) 177.
6. H. Zarrok, H. Oudda, A. Zarrouk, R. Salghi, B. Hammouti, M. Bouachrine, *Der Pharm. Chem.* 3 (2011) 576.
7. H. Zarrok, R. Salghi, A. Zarrouk, B. Hammouti, H. Oudda, Lh. Bazzi, L. Bammou, S. S. Al-Deyab, *Der Pharm. Chem.* 4 (2012) 407.
8. H. Zarrok, S. S. Al-Deyab, A. Zarrouk, R. Salghi, B. Hammouti, H. Oudda, M. Bouachrine, F. Bentiss, *Int. J. Electrochem. Sci.* 7 (2012) 4047.
9. D. Ben Hmamou, R. Salghi, A. Zarrouk, H. Zarrok, B. Hammouti, S. S. Al-Deyab, M. Bouachrine, A. Chakir, M. Zougagh, *Int. J. Electrochem. Sci.* 7 (2012) 5716.
10. A. Zarrouk, B. Hammouti, S.S. Al-Deyab, R. Salghi, H. Zarrok, C. Jama, F. Bentiss, *Int. J. Electrochem. Sci.* 7 (2012) 5997.
11. A. Zarrouk, H. Zarrok, R. Salghi, B. Hammouti, S.S. Al-Deyab, R. Touzani, M. Bouachrine, I. Warad, T. B. Hadda, *Int. J. Electrochem. Sci.* 7 (2012) 6353.
12. A. Zarrouk, M. Messali, H. Zarrok, R. Salghi, A. Al-Sheikh Ali, B. Hammouti, S. S. Al-Deyab, F. Bentiss, *Int. J. Electrochem. Sci.* 7 (2012) 6998.
13. H. Zarrok, A. Zarrouk, R. Salghi, Y. Ramli, B. Hammouti, S. S. Al-Deyab, E. M. Essassi, H. Oudda, *Int. J. Electrochem. Sci.* 7 (2012) 8958.
14. D. Ben Hmamou, R. Salghi, A. Zarrouk, H. Zarrok, S. S. Al-Deyab, O. Benali, B. Hammouti, *Int. J. Electrochem. Sci.* 7 (2012) 8988.
15. A. Zarrouk, M. Messali, M. R. Aouad, M. Assouag, H. Zarrok, R. Salghi, B. Hammouti, A. Chetouani, *J. Chem. Pharm. Res.* 4 (2012) 3427.
16. D. Ben Hmamou, M. R. Aouad, R. Salghi, A. Zarrouk, M. Assouag, O. Benali, M. Messali, H. Zarrok, B. Hammouti, *J. Chem. Pharm. Res.* 4 (2012) 3489.
17. H. Zarrok, H. Oudda, A. El Midaoui, A. Zarrouk, B. Hammouti, M. Ebn Touhami, A. Attayibat, S. Radi, R. Touzani, *Res. Chem. Intermed* (2012) DOI 10.1007/s11164-012-0525-x
18. A. Zarrouk, B. Hammouti, H. Zarrok, R. Salghi, A. Dafali, Lh. Bazzi, L. Bammou, S. S. Al-Deyab, *Der Pharm. Chem.* 4 (2012) 337

19. A. Zarrouk, A. Dafali, B. Hammouti, H. Zarrok, S. Boukhris, M. Zertoubi, *Int. J. Electrochem. Sci.* 5 (2010) 46.
20. A. Zarrouk, T. Chelfi, A. Dafali, B. Hammouti, S.S. Al-Deyab, I. Warad, N. Benchat, M. Zertoubi, *Int. J. Electrochem. Sci.* 5 (2010) 696.
21. A. Zarrouk, I. Warad, B. Hammouti, A. Dafali, S.S. Al-Deyab, N. Benchat, *Int. J. Electrochem. Sci.* 5 (2010) 1516.
22. A. Zarrouk, B. Hammouti, R. Touzani, S.S. Al-Deyab, M. Zertoubi, A. Dafali, S. Elkadiri, *Int. J. Electrochem. Sci.* 6 (2011) 4939.
23. A. Zarrouk, B. Hammouti, H. Zarrok, S.S. Al-Deyab, M. Messali, *Int. J. Electrochem. Sci.* 6 (2011) 6261.
24. X. Li, S. Deng, H. Fu, *Corros. Sci.* 53 (2011) 3704.
25. F. Ullmann, *Chem. Ber.* 36, (1903), 2384.
26. F. Ullig *Angew. Chem.* 15, (1954), 435.
27. A.D. Becke. *J. Chem. Phys.* 96 (1992) 9489.
28. A.D. Becke. *J. Chem. Phys.* 98 (1993) 1372.
29. C. Lee, W. Yang, R.G. Parr. *Phys. Rev. B.* 37 (1988) 785.
30. Gaussian 03, Revision B.01, M. J. Frisch, et al., Gaussian, Inc., Pittsburgh, PA, (2003).
31. S.S. Abdel-Rehim, M.A.M. Ibrahim, K.F. Khaled, *Mater. Chem. Phys.* 70 (2001) 268.
32. Z. Tao, S. Zhang, W. Li, B. Hou, *Corros. Sci.* 51 (2009) 2588.
33. A.Y. Musa, A.A.H. Kadhum, A.B. Mohamad, M.S. Takriff, *Corros. Sci.* 52 (2010) 3331.
34. J. Zhang, X.L. Gong, H.H. Yu, M. Du, *Corros. Sci.* 53 (2011) 3324.
35. C.H. Hsu, F. Mansfeld, *Corrosion.* 57 (2001) 747.
36. E. Machnikova, K.H. Whitmire, N. Hackerman, *Electrochim. Acta* 53 (2008) 6024.
37. G. Avci, *Mater. Chem. Phys.* 112 (2008) 234.
38. K.F. Khaled, *Mater. Chem. Phys.* 112 (2008) 290.
39. M. Behpour, S.M. Ghoreishi, N. Mohammadi, N. Soltani, M. Salavati-Niasari, *Corros. Sci.* 52 (2010) 4046.
40. E.S. Ferreira, C. Giancomlli, F.C. Giacomlli, A. Spinelli, *Mater. Chem. Phys.* 83 (2004) 129
41. L.J.M. Vrac̃ar, D.M. Draz̃ic, *Corros. Sci.* 44 (2002) 16.
42. S.M.A. Hosseini, M. Salari, E. Jamalizadeh, S. Khezripor, M. Seifi, *Mater. Chem. Phys.* 119 (2010) 100.
43. X.H. Li, S.D. Deng, *Corros. Sci.* 509 (2008) 420
44. L. Narvaez, E. Cano, D.M. Bastidas, *J. Appl. Electrochem.* 35 (2005) 499.
45. X. Li, S. Deng, H. Fu, *Corros. Sci.* 53 (2011) 664.
46. S. Deng, X. Li, H. Fu, *Corros. Sci.* 53 (2011) 760.
47. B. Hammouti, A. Zarrouk, S.S. Al-Deyab And I. Warad, *Orient. J. Chem.*, 27 (2011) 23.
48. L. Herrag, A. Chetouani, B. Hammouti, A. Aouniti, A. Zarrouk, S. El Kadiri, *Der Pharm. Chem.*, 4(4) (2012) 1522.
49. S. Rekkab, H. Zarrok, R. Salghi, A. Zarrouk, Lh. Bazzi, B. Hammouti, Z. Kabouche, R. Touzani, M. Zougagh, *J. Mater. Environ. Sci.* 3 (4) (2012) 613.
50. M.A., Migahed and I.F. Nassar, *Electrochim. Acta*, 53 (2008) 2877.
51. S.S. Abd El-Rehim, H.H. Hassan, and M.A. Amin, *Mater. Chem. Phys.*, 70 (2001) 64
52. M.M. Osman, A.M.A. Omar, and A.M. El-Sabagh, *Mater. Chem. Phys.*, 50 (1997) 271.
53. L. Bammou, R. Salghi, A. Zarrouk, H. Zarrok, S. S. Al-Deyab, B. Hammouti, M. Zougagh, M. Errami, *Int. J. Electrochem. Sci.*, 7 (2012) 8974.
54. H. Zarrok, A. Zarrouk, B. Hammouti, R. Salghi, C. Jama, F. Bentiss, *Corros. Sci.* 64 (2012) 243.
55. L. Narvaez, E. Cano, D.M. Bastidas, *J. Appl. Electrochem.* 35 (2005) 499.
56. A. Ghazoui, R. Saddik, N. Benchat, M. Guenbour, B. Hammouti, S.S. Al-Deyab, A. Zarrouk, *Int. J. Electrochem. Sci.*, 7 (2012) 7080.
57. R. Agrawal, T.K.G. Namboodhiri, *Corros. Sci.* 30 (1990) 37.

58. M.A. Migahed, A.A. Farag, S.M. Elsaed, R. Kamal, M. Mostfa, H. Abd El-Bary, *Mater. Chem. Phys.* 125 (2011) 125.
59. K. Mallaiyaa, R. Subramaniama, S.S. Srikandana, S. Gowria, N. Rajasekaranb, A. Selvaraj, *Electrochim. Acta*, 56 (2011) 3857.
60. G.K. Gomma, M.H. Wahdan, *Bull. Chem. Soc. Jpn.* 67 (1994) 1.
61. H. Ashassi-Sorkhabi, B. Shabani, B. Aligholipour, D. Seifzadeh, *Appl. Surf. Sci.* 252(2006) 4047.
62. G. Avci, *Colloid. Surf. A.* 317 (2008) 730.
63. S.M.A. Hosseini, A. Azimi, *Corros. Sci.* 51 (2009) 728. F. B. Growcock, *Corrosion.*, 45 (1989) 1003.
64. F. B. Growcock, *Corrosion.*, 45 (1989) 1003.
65. A. Domenicano, I. Hargittai, *Accurate Molecular Structures, Their Determination and Importance*, Oxford University Press, New York, (1992).
66. M. J. S. Dewar, W. Thiel, *J. Am. Chem. Soc.*, 99 (1977) 4899.
67. A.Y. Musa, A. H. Kadhun, A. B. Mohamad, A.b. Rohoma, H. Mesmari, *J. Mol. Struct.*, 969 (2010) 233.
68. M.A. Amin, K.F. Khaled, S.A. Fadi-Allah, *Corros. Sci.*, 52 (2010) 140.
69. G. Gece, S. Bilgic, *Corros. Sci.*, 51 (2009) 1876.
70. E.E. Ebenso, D.A. Isabirye, N.O. Eddy, *Int. J. Mol. Sci.*, 11 (2010) 2473.
71. O. Kikuchi, *Quant. Struct.-Act. Relat.*, 6 (1987) 179
72. H. Ju, Z.P. Kai, Y. Li, *Corros. Sci.*, 50 (2008) 865.